

4-(2-Tetrathiafulvalenyl-ethenyl)pyridine (TTF–CH=CH–Py) Radical Cation Salts Containing Poly(β -diketonate) Rare Earth Complexes: Synthesis, Crystal Structure, Photoluminescent and Magnetic Properties

Fabrice Pointillart,[†] Olivier Maury,[‡] Yann Le Gal,[†] Stéphane Golhen,[†] Olivier Cador,[†] and Lahcène Ouahab^{*†}

[†]Organométalliques et Matériaux Moléculaires, UMR 6226 CNRS-URI Sciences Chimiques de Rennes, Université de Rennes 1, 35042 Rennes Cedex, France, and [‡]Université de Lyon, ICL-CNRS Ecole Normale Supérieure de Lyon UMR 5182, 46 Allée d'Italie, 69364 Lyon Cedex 07, France

Received June 1, 2009

The reactions between the redox-active 4-(2-tetrathiafulvalenyl-ethenyl)pyridine ligand (TTF–CH=CH–Py) and the tris(1,1,1,5,5,5-hexafluoroacetylacetonate)Ln(III) (Ln = La and Nd) lead to the formation of compounds with the formulas $\{[\text{La}(\text{hfac})_5][(\text{TTF}-\text{CH}=\text{CH}-\text{Py}^{\bullet+})]_2\}$ (**1**), $\{[\text{Nd}(\text{hfac})_4(\text{H}_2\text{O})][(\text{TTF}-\text{CH}=\text{CH}-\text{Py}^{\bullet+})]_2\}$ (**2**), and $\{[\text{Nd}(\text{hfac})_4(\text{H}_2\text{O})][(\text{TTF}-\text{CH}=\text{CH}-\text{Py}^{\bullet+})]_2(\text{C}_6\text{H}_{14})_{0.5}\}$ (**3**) (hfac[−] = 1,1,1,5,5,5-hexafluoroacetylacetonate anion). These compounds have been characterized by single-crystal X-ray diffraction, optical, and magnetic measurements. Compounds **1**, **2**, and **3** crystallize in the monoclinic *C2/c*, triclinic *P1̄*, and monoclinic *P2₁/c* space groups, respectively. La(III) adopts a tetradecahedral geometry, while Nd(III) stands in a distorted capped square antiprism one. In **1**, the inorganic network is formed by the $[\text{La}(\text{hfac})_5]^{2-}$ dianionic complexes, while it is formed by a pseudo-dimeric dianionic unit of formula $\{[\text{Nd}(\text{hfac})_4(\text{H}_2\text{O})]_2\}^{2-}$ in **2** and **3**. In all crystal structures, the organic network is constituted by the TTF–CH=CH–Py^{•+} radical cations. The inorganic and organic networks interact through intermolecular contacts between the pyridine moieties of the TTF–CH=CH–Py^{•+} radical cations and the Ln(III) ions. The luminescence properties of the Nd(III) ions (9400 cm^{−1}) and fluorescence band of the TTF–CH=CH–Py^{•+} radical cations (10200 cm^{−1}) have been observed and studied for compound **2**. Complexes **2** and **3** are paramagnetic because of Nd(III) ions. Compound **2** is a paramagnetic luminescent TTF-radical-cation-based material. Resistivity measurements have also been performed on these materials.

Introduction

In the past decade, multifunctional materials which possess magnetic and electrical properties have emerged.^{1–3} A lot of molecular compounds that consist of organic donors and paramagnetic anions have been studied.⁴ Some of them are paramagnetic metals, while others are paramagnetic superconductors.¹ Moreover, in some compounds, the conducting

electrons are coupled with the localized unpaired electrons, resulting in a wide variety of cooperative phenomena.^{5–10} These materials are called “ π -d systems” because they consist of delocalized π and localized d electrons in which novel transport properties have been found, such as successive transitions from paramagnetic-metal to antiferromagnetic-metal and finally to an antiferromagnetic-superconductor or magnetic-field-induced superconducting transition.^{11,12} The π -d interactions can occur through space,

*To whom correspondence should be addressed. E-mail: Lahcene.Ouahab@univ-rennes1.fr.

(1) (a) Kurmoo, M.; Graham, A. W.; Day, P.; Coles, S. J.; Hurtsthouse, M. B.; Cauffman, J. M.; Singleton, J.; Ducasse, L.; Guionneau, P. *J. Am. Chem. Soc.* **1995**, *117*, 12209. (b) Coronado, E.; Day, P. *Chem. Rev.* **2004**, *104*, 5419.

(2) (a) Kobayashi, H.; Tomita, H.; Naito, T.; Kobayashi, A.; Sakai, F.; Watanabe, T.; Cassoux, P. *J. Am. Chem. Soc.* **1996**, *118*, 368. (b) Ouahab, L.; Enoki, T. *Eur. J. Inorg. Chem.* **2004**, 933.

(3) (a) Coronado, E.; Galán-Mascarós, J. R.; Gomes-García, C. J.; Laukhin, V. *Nature* **2000**, *408*, 447. (b) Enoki, T.; Miyasaki, A. *Chem. Rev.* **2004**, *104*, 5449.

(4) (a) Kobayashi, H.; Kobayashi, A.; Cassoux, P. *Chem. Soc. Rev.* **2000**, *29*, 325. (b) Kobayashi, A.; Fujiwara, E.; Kobayashi, H. *Chem. Rev.* **2004**, *104*, 5243.

(5) Ojima, E.; Fujiwara, H.; Kato, K.; Kobayashi, H.; Tanaka, H.; Kobayashi, A.; Tokumoto, M.; Cassoux, P. *J. Am. Chem. Soc.* **1999**, *121*, 5581.

(6) Fujiwara, H.; Ojima, E.; Nakazawa, Y.; Narymbetov, B. Zh.; Kato, K.; Kobayashi, H.; Kobayashi, A.; Tokumoto, M.; Cassoux, P. *J. Am. Chem. Soc.* **2001**, *123*, 306.

(7) Otsuka, T.; Kobayashi, A.; Miyamoto, Y.; Kiuchi, J.; Wada, N.; Ojima, E.; Fujiwara, F.; Kobayashi, H. *Chem. Lett.* **2000**, 732.

(8) Otsuka, T.; Kobayashi, A.; Miyamoto, Y.; Kiuchi, J.; Nakamura, S.; Wada, N.; Fujiwara, E.; Fujiwara, H.; Kobayashi, H. *J. Solid State Chem.* **2001**, *159*, 407.

(9) Kobayashi, H.; Sato, A.; Arai, E.; Akutsu, H.; Kobayashi, A.; Cassoux, P. *J. Am. Chem. Soc.* **1997**, *119*, 12392.

(10) Sato, A.; Ojima, E.; Akutsu, H.; Nakazawa, Y.; Kobayashi, H.; Tanaka, H.; Kobayashi, A.; Cassoux, P. *Chem. Lett.* **1998**, 673.

(11) Tanaka, H.; Kobayashi, H.; Kobayashi, A.; Cassoux, P. *Adv. Mater.* **2000**, *12*, 1685.

(12) Uji, S.; Shinagawa, H.; Terashima, T.; Terakura, C.; Yakabe, T.; Terai, Y.; Tokumoto, M.; Kobayashi, A.; Tanaka, H.; Kobayashi, H. *Nature* **2001**, *410*, 908.

and should therefore be weak, or through a conjugated bridge.^{13–36} In this latter case, the π and d systems are covalently linked. To elaborate on such a system, the redox-active 4-(2-tetrathiafulvalenyl-ethenyl)pyridine ligand (TTF–CH=CH–Py) has been synthesized.³⁷ It has been successfully coordinated (in a neutral,²⁹ partially oxidized,³⁸ or fully oxidized³⁹ form) to Cu(II) (3d), and very recently, coordination to Ru(III) (4d) has been realized.⁴⁰ The f block elements, namely, lanthanides, show peculiar magnetic properties with respect to d block elements. The inner f electrons (the spin carriers) are well-shielded by outer closed-shell electrons, and the spin–orbit coupling is considered to play an essential role in their magnetic properties. Another exciting possibility is the use of specific luminescent properties of lanthanides in addition to their magnetism. For example, lanthanide complexes with β -diketones have garnered a large amount of attention⁴¹ over the past three decades due to

their potential applications in the design of chelate lasers,⁴² efficient organic light-emitting diodes,⁴³ and polymer light-emitting diodes,⁴⁴ as NMR shift reagents⁴⁵ in analytical applications, and as modern antibody catalysts in biochemistry.⁴⁶ Most of the hitherto studied rare-earth β -diketonate complexes belong to a group of tris complexes of the type $M(\beta\text{-diketone})_3L$ or $M(\beta\text{-diketone})_3L_2$. Here, the two unoccupied coordination positions are usually filled up by additional neutral organic ligands L, which can serve as an antenna, providing an efficient pathway for excitation of the lanthanide ion. The emission of the lanthanide center can be sensitized thanks an iridium- or platinum-based complex. In this way, some Ir–Eu heterobimetallic compounds have been reported.⁴⁷ Though the molecular metals incorporating localized f electrons are still very limited,^{48–51} the study of the “ π –f system” will undoubtedly expand the range of multifunctional molecular materials. One of the reasons why these materials have not been much explored is due to the fact that lanthanides form anionic complexes that are much larger in size and charge compared with the d block elements, so good crystallinity is difficult to achieve.

In the following, we report the reactions we have performed between the redox-active TTF–CH=CH–Py potential ligand and two Ln(III)(hfac)₃ complexes (Ln = La and Nd, hfac = 1,1,1,5,5,5-hexafluoroacetylacetonate). These reactions lead to the three radical donor salts containing poly(β -diketone)Ln(III), which are formulated as $\{[La(hfac)_3][(TTF-CH=CH-Py^+)]_2\}$ (1), $\{[Nd(hfac)_4(H_2O)][(TTF-CH=CH-Py^+)]_2\}$ (2), and $\{[Nd(hfac)_4(H_2O)][(TTF-CH=CH-Py^+)]_2(H_2O)-(C_6H_{14})_{0.5}\}$ (3). Compounds 1, 2, and 3 have been characterized by single-crystal X-ray diffraction, IR spectroscopy, absorption UV–visible spectroscopy, luminescence, electron paramagnetic resonance (EPR), superconducting quantum interference device (SQUID), and resistivity measurements.

Experimental Section

Synthesis. General Procedures and Materials. All solvents were dried using standard procedures. The precursors Ln(hfac)₃·3H₂O (Ln = La and Nd;⁵² hfac[−] = 1,1,1,5,5,5-hexafluoroacetylacetonate anion) and 4-(2-tetrathiafulvalenyl-ethenyl)pyridine (TTF–CH=CH–Py)³⁷ were synthesized following previously reported methods. All other reagents were

- (13) Bouguessa, S.; Gouasmia, A. K.; Golhen, S.; Ouahab, L.; Fabre, J.-M. *Tetrahedron Lett.* **2003**, *44*, 9275.
 (14) Liu, S.-X.; Dolder, S.; Rusanov, E. B.; Stoeckli-Evans, H.; Decurtins, S. C. R. *Chim.* **2003**, *6*, 657.
 (15) Liu, S.-X.; Dolder, S.; Pilkington, M.; Decurtins, S. J. *Org. Chem.* **2002**, *67*, 3160.
 (16) Jia, C.; Zhang, D.; Xu, Y.; Xu, W.; Hu, U.; Zhu, D. *Synth. Met.* **2003**, *132*, 249.
 (17) Becher, J.; Hazell, A.; McKenzie, C. J.; Vestergaard, C. *Polyhedron* **2000**, *19*, 665.
 (18) Devic, T.; Avarvari, N.; Batail, P. *Chem.—Eur. J.* **2004**, *10*, 3697.
 (19) Ota, A.; Ouahab, L.; Golhen, S.; Cador, O.; Yoshida, Y.; Saito, G. *New. J. Chem.* **2005**, *29*, 1135.
 (20) Liu, S.-X.; Dolder, S.; Franz, P.; Neels, A.; Stoeckli-Evans, H.; Decurtins, S. *Inorg. Chem.* **2003**, *42*, 4801.
 (21) Xue, H.; Tang, X.-J.; Wu, L.-Z.; Zhang, L.-P.; Tung, C.-H. *J. Org. Chem.* **2005**, *70*, 9727.
 (22) Benbellat, N.; Le Gal, Y.; Golhen, S.; Gouasmia, A.; Ouahab, L.; Fabre, J.-M. *Eur. J. Org. Chem.* **2006**, 4237.
 (23) Hervé, K.; Liu, S.-X.; Cador, O.; Golhen, S.; Le Gal, Y.; Bousseksou, A.; Stoeckli-Evans, H.; Decurtins, S.; Ouahab, L. *Eur. J. Inorg. Chem.* **2006**, 3498.
 (24) Massue, J.; Bellec, N.; Chopin, S.; Levillain, E.; Roisnel, T.; Clérac, R.; Lorcy, D. *Inorg. Chem.* **2005**, *44*, 8740.
 (25) Pellon, P.; Gachot, G.; Le Bris, J.; Marchin, S.; Carlier, R.; Lorcy, D. *Inorg. Chem.* **2003**, *43*, 2056.
 (26) Smucker, B. W.; Dunbar, K. R. J. *J. Chem. Soc., Dalton Trans.* **2000**, 1309.
 (27) Devic, T.; Batail, P.; Fourmigué, M.; Avarvari, N. *Inorg. Chem.* **2004**, *43*, 3136.
 (28) Avarvari, N.; Fourmigué, M. *Chem. Commun.* **2004**, 1300.
 (29) Iwahori, F.; Golhen, S.; Ouahab, L.; Carlier, R.; Sutter, J.-P. *Inorg. Chem.* **2001**, *40*, 6541.
 (30) Ouahab, L.; Iwahori, F.; Golhen, S.; Carlier, R.; Sutter, J.-P. *Synth. Met.* **2003**, *133–134*, 505.
 (31) Jia, C.; Liu, S.-X.; Ambrus, C.; Neels, A.; Labat, G.; Decurtins, S. *Inorg. Chem.* **2006**, *45*, 3152.
 (32) Ichikawa, S.; Kimura, S.; Mori, H.; Yoshida, G.; Tajima, H. *Inorg. Chem.* **2006**, *45*, 7575.
 (33) Wang, L.; Zhang, B.; Zhang, J. *Inorg. Chem.* **2006**, *45*, 6860.
 (34) Gavrilenko, K. S.; Le Gal, Y.; Cador, O.; Golhen, S.; Ouahab, L. *Chem. Commun.* **2007**, 280.
 (35) Chahma, M.; Hassan, N.; Alberola, A.; Stoeckli-Evans, H.; Pilkington, M. *Inorg. Chem.* **2007**, *46*, 3807.
 (36) Wu, J.-C.; Liu, S.-X.; Keene, T. D.; Neels, A.; Mereacre, V.; Powell, A. K.; Decurtins, S. *Inorg. Chem.* **2008**, *47*, 3452.
 (37) Andreu, R.; Malfant, I.; Lacroix, P. G.; Cassoux, P. *J. Eur. Org. Chem.* **2000**, 737.
 (38) Setifi, F.; Ouahab, L.; Golhen, S.; Yoshida, Y.; Saito, G. *Inorg. Chem.* **2003**, *42*, 1791.
 (39) Hervé, K.; Le Gal, Y.; Ouahab, L.; Golhen, S.; Cador, O. *Synth. Met.* **2005**, *153*, 461.
 (40) Pointillart, F.; Le Gal, Y.; Golhen, S.; Cador, O.; Ouahab, L. *Inorg. Chem.* **2008**, *47*, 9730.
 (41) (a) Horrocks De, W. W. Jr.; Bolender, P.; Smith, W. D.; Supkowski, R. M. *J. Am. Chem. Soc.* **1997**, *119*, 5972. (b) De Bettencourt-Dias, A. *Dalton Trans.* **2007**, 2229. (c) Kido, J.; Okamoto, Y. *Chem. Rev.* **2002**, *102*, 2357.
 (42) Lempicki, A.; Samelson, H. *Phys. Lett.* **1963**, *4*, 133.

(43) Tang, C. W.; Vanslyka, S. A. *Appl. Phys. Lett.* **1987**, *51*, 2902.

(44) Burroughes, J. H.; Bradley, D. D. C.; Holmes, A. B. *Nature* **1990**, *347*, 539.

(45) Wenzel, T. J. In *Lanthanide Shift Reagents in Stereochemical Analysis*; Morrill, T. C., Ed.; VCH Publishers: Weinheim, Germany, 1986; pp 151–173, Chapter 5.

(46) Hemmilla, I. A. *Application of Fluorescence in Immunoassays*; Wiley: New York, 1991.

(47) (a) Chen, F.-F.; Bian, Z.-Q.; Liu, Z.-W.; Nie, D.-B.; Chen, Z.-Q.; Huang, C.-H. *Inorg. Chem.* **2008**, *47*, 2507. (b) Xu, H.-B.; Shi, L.-X.; Ma, E.; Zhang, L.-Y.; Wei, Q.-H.; Chen, Z.-N. *Chem. Commun.* **2006**, 1601. (c) Coppo, P.; Duati, M.; Kozhevnikov, V. N.; Hofstraat, J. W.; De Cola, L. *Angew. Chem., Int. Ed.* **2005**, *44*, 1806.

(48) Imakubo, T.; Sawa, H.; Tajima, H.; Kato, R. *Synth. Met.* **1997**, *86*, 2047.

(49) Tamura, M.; Matsuzaki, F.; Nishio, Y.; Kajita, K.; Kitazawa, T.; Mori, H.; Tanaka, S. *Synth. Met.* **1999**, *102*, 1716.

(50) Dyachenko, O. A.; Kazheva, O. N.; Gritsenko, V. V.; Kuschch, N. D. *Synth. Met.* **2001**, *120*, 1017.

(51) (a) Faulkner, S.; Burton-Pye, B. P.; Khan, T.; Martin, L. R.; Wray, S. D.; Skabara, P. J. *Chem. Commun.* **2002**, *16*, 1668. (b) Pointillart, F.; Le Gal, Y.; Golhen, S.; Cador, O.; Ouahab, L. *Inorg. Chem.* DOI: 10.1021/ic9003966.

(52) Richardson, M. F.; Wagner, W. F.; Sands, D. E. *J. Inorg. Nucl. Chem.* **1968**, *30*, 1275.

Table 1. X-Ray Crystallographic Data for $\{[\text{La}(\text{hfac})_3][(\text{TTF}-\text{CH}=\text{CH}-\text{Py}^+)]_2\}$ (**1**), $\{[\text{Nd}(\text{hfac})_4(\text{H}_2\text{O})][(\text{TTF}-\text{CH}=\text{CH}-\text{Py}^+)]_2\}$ (**2**), and $\{[\text{Nd}(\text{hfac})_4(\text{H}_2\text{O})][(\text{TTF}-\text{CH}=\text{CH}-\text{Py}^+)]_2(\text{H}_2\text{O})(\text{C}_6\text{H}_{14})_{0.5}\}$ (**3**)

compound	1	2	3
formula	$\text{C}_{51}\text{H}_{23}\text{N}_2\text{O}_{10}\text{S}_8\text{F}_{30}\text{La}$	$\text{C}_{66}\text{H}_{30}\text{N}_2\text{O}_{18}\text{S}_8\text{F}_{48}\text{Nd}_2$	$\text{C}_{69}\text{H}_{39}\text{N}_2\text{O}_{19}\text{S}_8\text{F}_{48}\text{Nd}_2$
M/g mol ⁻¹	1789.1	2595.88	2656.4
cryst syst	monoclinic	triclinic	monoclinic
space group	$C2/c$ (No. 15)	$P\bar{1}$ (No. 2)	$P2_1/c$ (No. 14)
unit cell parameters	$a = 36.2646(13) \text{ \AA}$ $b = 19.0458(8) \text{ \AA}$ $c = 22.0307(4) \text{ \AA}$ $\beta = 115.236(2)^\circ$	$a = 16.9290(8) \text{ \AA}$ $b = 17.4612(7) \text{ \AA}$ $c = 20.1786(9) \text{ \AA}$ $\alpha = 97.421(2)^\circ$ $\beta = 109.498(2)^\circ$ $\gamma = 107.129(2)^\circ$	$a = 23.9926(3) \text{ \AA}$ $b = 12.1328(2) \text{ \AA}$ $c = 34.3105(4) \text{ \AA}$ $\beta = 91.342(1)^\circ$
volume/ \AA^3	13764.1(8)	5199.2(4)	9985.0(2)
cell formula units	$Z = 8$	$Z = 2$	$Z = 4$
T/K	293 (2)	293 (2)	293 (2)
diffraction refln	$2.48^\circ \leq 2\theta \leq 51.38^\circ$	$4.96^\circ \leq 2\theta \leq 50.60^\circ$	$4.90^\circ \leq 2\theta \leq 54.96^\circ$
$\rho_{\text{calcd}}/\text{g cm}^{-3}$	1.727	1.658	1.763
μ/mm^{-1}	0.998	1.290	1.346
number of reflns	20651	35356	43330
independent reflns	12325	17751	22776
$I > 2\sigma(I)$	8182	10733	10476
number of variables	919	1409	1333
$R_{\text{int}}, R_1, wR_2$	0.0342, 0.0764, 0.2155	0.0454, 0.0642, 0.1742	0.0786, 0.0708, 0.1852

purchased from Aldrich Co., Ltd. and were used without further purification.

Synthesis of Complexes 1, 2, and 3. $\{[\text{La}(\text{hfac})_3][(\text{TTF}-\text{CH}=\text{CH}-\text{Py}^+)]_2\}$ (**1**). $\text{La}(\text{hfac})_3 \cdot 3\text{H}_2\text{O}$ (30.6 mg, 0.037 mmol) was added to boiling *n*-heptane (15 mL), and the solution was stirred for 10 min and cooled to 70 °C. Then, $\text{TTF}-\text{CH}=\text{CH}-\text{Py}$ (23.1 mg, 0.075 mmol) in CH_2Cl_2 (10 mL) was added to the hot *n*-heptane solution, and the stirring continued for 15 min. Immediately after the addition, the solution turned dark blue. Slow evaporation of the resulting solution for one night at 4 °C gave dark blue block-shaped crystals of **1**, suitable for X-ray diffraction analysis, and an uncharacterized green-gray powder. Yield: 20 mg (30%). IR (KBr): ν 3261, 3155, 3092, 1653, 1600, 1557, 1533, 1508, 1492, 1259, 1201, 1145, 1095, 799, 661, 585 cm^{-1} . Anal. Calcd (%) for $\text{C}_{51}\text{H}_{23}\text{N}_2\text{O}_{10}\text{S}_8\text{F}_{30}\text{La}$: C, 34.21; H, 1.29; N, 1.57. Found: C, 33.79; H, 1.23; N, 1.42.

$\{[\text{Nd}(\text{hfac})_4(\text{H}_2\text{O})][(\text{TTF}-\text{CH}=\text{CH}-\text{Py}^+)]_2\}$ (**2**). This compound was synthesized by a procedure similar to that used for **1** starting from $\text{Nd}(\text{hfac})_3 \cdot 3\text{H}_2\text{O}$ (30.8 mg, 0.037 mmol) and $\text{TTF}-\text{CH}=\text{CH}-\text{Py}$ (23.1 mg, 0.075 mmol). Dark blue block-shaped single crystals were obtained by slow evaporation of a CH_2Cl_2 /heptane solution of **2** at room temperature. Yield: 15 mg (31%). IR (KBr): ν 3253, 3165, 3098, 1658, 1598, 1555, 1493, 1257, 1200, 1144, 1092, 790, 660, 583 cm^{-1} . Anal. Calcd (%) for $\text{C}_{66}\text{H}_{30}\text{N}_2\text{O}_{18}\text{S}_8\text{F}_{48}\text{Nd}_2$: C, 30.51; H, 1.16; N, 1.08. Found: C, 30.79; H, 1.23; N, 1.02.

$\{[\text{Nd}(\text{hfac})_4(\text{H}_2\text{O})][(\text{TTF}-\text{CH}=\text{CH}-\text{Py}^+)]_2(\text{H}_2\text{O})(\text{C}_6\text{H}_{14})_{0.5}\}$ (**3**). This compound was synthesized by a similar procedure to that used for **2** starting from 11.6 mg of $\text{TTF}-\text{CH}=\text{CH}-\text{Py}$ (0.037 mmol). Dark blue single crystals were obtained by slow evaporation of a CH_2Cl_2 /hexane solution of **3** at 4 °C. Yield: 51 mg (51%). IR (KBr): ν 3250, 3164, 3098, 1657, 1599, 1551, 1493, 1257, 1199, 1145, 1092, 790, 658, 580 cm^{-1} . Anal. Calcd (%) for $\text{C}_{69}\text{H}_{39}\text{N}_2\text{O}_{19}\text{S}_8\text{F}_{48}\text{Nd}_2$: C, 31.17; H, 1.47; N, 1.05. Found: C, 30.69; H, 1.28; N, 1.07.

Structural and Physical Measurements. Single crystals were mounted on a Nonius four-circle diffractometer equipped with a CCD camera and a graphite monochromated Mo $K\alpha$ radiation source ($\lambda = 0.71073 \text{ \AA}$), from the Centre de Diffraction (CDFIX), Université de Rennes 1, France. Data were collected at 293 K. Structures were solved with a direct method using the

SIR-97 program and refined with a full matrix least-squares method on F^2 using the SHELXL-97 program.^{53,54} Despite all structures containing solvent-accessible voids, no SQUEEZE procedure was performed. Crystallographic data are summarized in Table 1. Complete crystal structure results, in CIF file format, including bond lengths, angles, and atomic coordinates are provided in the Supporting Information. Optical spectra were measured using the KBr disk method on Perkin-Elmer 1600 Series FT-IR (resolution 4 cm^{-1}) for infrared. Absorption spectra were recorded using the KBr disk method on a Varian Cary 5000 UV-visible-NIR spectrometer equipped with an integration sphere. The luminescence spectra were measured using a Horiba-Jobin Yvon Fluorolog-3 spectrofluorimeter, equipped with a three-slit double-grating excitation and emission monochromator with dispersions of 2.1 nm/mm (1200 grooves/mm). The steady-state luminescence was excited by unpolarized light from a 450 W xenon CW lamp and detected at an angle of 90° for diluted solution measurements or at 22.5° for solid-state measurement (front face detection) by a red-sensitive Hamamatsu R928 photomultiplier tube. Spectra were reference-corrected for both the excitation source light intensity variation (lamp and grating) and the emission spectral response (detector and grating). Uncorrected near-infrared spectra were recorded at an angle of 45° using a liquid-nitrogen-cooled, solid indium/gallium/arsenic detector (850–1600 nm). EPR spectra were recorded down to 67 K for crunched single crystals of **1**, **2**, and **3** with a BRUKER EMX X-band ESR spectrometer equipped with an OXFORD cryostat. The DC magnetic susceptibility measurements were performed on solid polycrystalline sample with a Quantum Design MPMS-XL SQUID magnetometer between 2 and 300 K in an applied magnetic field of 0.2 T for temperatures of 2–20 K and 1 T for temperatures of 20–300 K. These measurements were all corrected for the diamagnetic contribution, as calculated with Pascal's constants.

Results and Discussion

Synthesis. The reactions between the $\text{TTF}-\text{CH}=\text{CH}-\text{Py}$ ligand and $\text{Ln}(\text{hfac})_3 \cdot 3\text{H}_2\text{O}$ complexes ($\text{Ln} = \text{La}$ and Nd) at 70 °C lead to the formation of **1**, **2**, and **3**. For temperatures higher than 60 °C during the reaction, a change of color from red to dark blue is observed, which is related to the oxidation of the neutral $\text{TTF}-\text{CH}=\text{CH}-\text{Py}$ ligand to

(53) Otwinowski, Z.; Minor, W. Processing of X-ray Diffraction Data Collected in Oscillation Mode In *Methods in Enzymology, Volume 276: Macromolecular Crystallography, Part A*; Carter, C. W., Sweet, R. M., Jr., Eds.; Academic Press: New York, 1997; pp 307–326.

(54) Carter, C. W., Sweet, R. M., Jr. Eds.; Academic Press: 1997; pp 307–326.

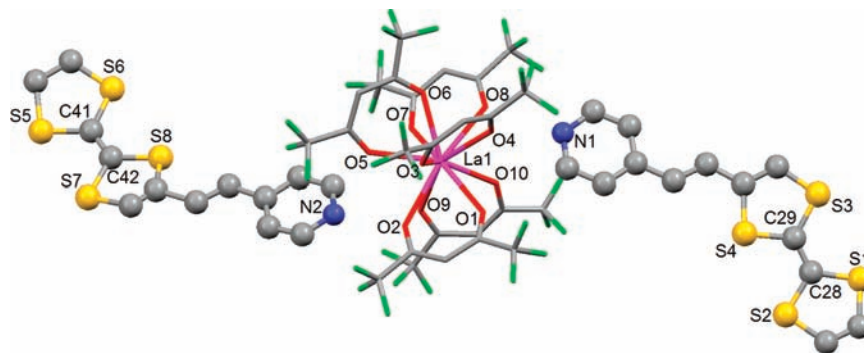


Figure 1. Representation of the asymmetric unit of **1**. The radical cation donors are drawn as balls and sticks; the anionic coordination complex of La(III) is drawn as capped sticks.

the radical one (TTF-CH=CH-Py^{•+}), whereas for temperatures lower than 60 °C, no oxidation or coordination of TTF-CH=CH-Py is observed. The oxidation also takes place under an argon atmosphere. The formation of the TTF radical derivative leads to a rearrangement around the lanthanide ion to keep a neutral charge for the compounds. The number of hfac⁻ anions coordinated to the lanthanide depends of its ionic radius. While the biggest lanthanides (La, Ce, Pr, and Nd) can form penta(bischelate ligands)Ln complexes,^{55–57} the smaller ones (Nd–Yb) form tetra-(bischelate ligands)Ln complexes.^{58–60} The case of the Nd(III) is intermediate because it can adopt octa-, nona-, and deca- coordinated geometries, but a study of the Cambridge crystallographic database shows that there are only two deposited tetrakis(β-diketonate)Nd(III) crystal structures and none with a TTF derivative radical salt. In any case, when *n*-heptane was used for the crystallization of the neodymium-based compounds, only **2** was obtained. The use of 2 equiv of TTF derivative for **2** optimizes the yield of the reaction. Finally, the responsible factor for the solvation of **3** is the nature of the solvent: when *n*-hexane was used for crystallization, compound **3** was obtained. There is no deposited crystal structure of a penta(β-diketonate)La(III) dianionic complex. These TTF derivative radical salts are obtained by an original chemical method because usually such salts are obtained by electrocrystallization.

Crystal Structures. {[La(hfac)₅][(TTF-CH=CH-Py^{•+})₂]} (**1**). Compound **1** crystallizes in the monoclinic C2/c (No. 15) space group (Table 1). An ORTEP view⁶¹ of the asymmetric unit is shown in Figure S1 (Supporting Information). It is composed of the penta(1,1,1,5,5,5-hexafluoroacetylacetonate)La(III) dianionic complex (drawn as capped sticks in Figure 1) and two TTF-CH=CH-Py^{•+} radical cations (drawn as balls and sticks

Table 2. Selected Bond Lengths (Å) and Intermolecular Distances for **1**, **2**, and **3**^a

	1	2	3
La1–O1	2.554(6)	Nd1–O1	2.485(5)
La1–O2	2.652(6)	Nd1–O2	2.468(6)
La1–O3	2.563(6)	Nd1–O3	2.416(7)
La1–O4	2.569(5)	Nd1–O4	2.459(6)
La1–O5	2.557(5)	Nd1–O5	2.487(5)
La1–O6	2.561(5)	Nd1–O6	2.415(6)
La1–O7	2.526(6)	Nd1–O7	2.529(6)
La1–O8	2.688(6)	Nd1–O8	2.489(5)
La1–O9	2.616(5)	Nd1–O9w	2.553(9)
La1–O10	2.544(6)	Nd2–O10	2.404(6)
La1–N1 ⁱ	4.378(8)	Nd2–O11	2.477(6)
La1–N2	4.409(8)	Nd2–O12	2.497(6)
		Nd2–O13	2.534(6)
		Nd2–O14	2.443(6)
		Nd2–O15	2.400(7)
		Nd2–O16	2.482(6)
		Nd2–O17	2.488(6)
		Nd2–O18w	2.569(5)
		Nd1–N1 ⁱⁱ	4.018(9)
		Nd2–N2 ⁱⁱⁱ	4.003(8)
		Nd1–Nd1 ^{iv}	5.8297(9)
		Nd2–Nd2 ^v	5.7053(9)
		Nd1–Nd2	6.2253(6)

^aSymmetry used: (i) 0.5 – *x*, *y* – 0.5, 1.5 – *z*; (ii) *x* – 1, *y* – 1, *z*; (iii) 2 – *x*, 2 – *y*, 2 – *z*; (iv) –*x*, 1 – *y*, 1 – *z*; (v) 1 – *x*, –*y*, –*z*; (vi) 1 – *x*, –1.5 + *y*, 0.5 – *z*.

in Figure 1). The La(III) ion is surrounded by 10 oxygen atoms, which come from five bishelating hfac⁻ ligands. The La–O distances range from 2.526(6) to 2.688(6) Å (Table 2). A precise analysis of the La–O bond lengths shows that the three distances, involving the O2, O8, and O9 atoms, are longer than the others. This is due to the proximity of the TTF-CH=CH-Py^{•+} radical derivatives (Figure 1). The arrangement of the 10 coordinated oxygen atoms leads to a tetradecahedral polyhedron around the lanthanum, which is only very slightly distorted compared with the previously reported deca-coordinated [La(hfac)₃(bpy)₂] complex (bpy = 2,2′-bipyridine).⁵⁶ The mean value of the La–O distances (2.583(6) Å) in **1** is longer than in the [La(hfac)₃(bpy)₂] complex. The lower affinity of the lanthanum ion for nitrogen atoms compared to that for the oxygen ones leads to a contraction of the La–O bond lengths in [La(hfac)₃(bpy)₂]. In **1**, the electroneutrality is ensured by two TTF-CH=CH-Py^{•+} radical cations. However, the two TTF-CH=CH-Py^{•+} radicals not only are counter-anions in the crystal structure but interact with the lanthanide. In fact, the pyridyl groups of TTF cations are oriented toward the lanthanide to optimize the lanthanum–nitrogen

(55) Brown, T. L.; LeMay, H. E., Jr. *Chemistry: The Central Science*, 2nd ed.; Prentice-Hall: New York, 1981; p 191.

(56) Van Staveren, D. R.; Van Albada, G. A.; Haasnoot, J. G.; Kooijman, H.; Manotti Lanfredi, A. M.; Nieuwenhuizen, P. J.; Spek, A. L.; Uguzzoli, F.; Weyhermüller, T.; Reedijk, J. *Inorg. Chim. Acta* **2001**, *315*, 163.

(57) Pointillart, F. *Magnetism and Chirality: From the Tridimensional Oxalate Based Magnets to Verdazyl Based Chains*, Ph. D. thesis, Marie Curie University, Paris, France, **2005**.

(58) Sweeting, L. M.; Rheingold, A. L. *J. Am. Chem. Soc.* **1987**, *109*, 2652.

(59) Bennett, M. J.; Cotton, F. A.; Legzdins, P.; Lippard, J. *Inorg. Chem.* **1968**, *7*, 1770.

(60) Binnemans, K. *Handbook on the Physics and Chemistry of Rare Earths*; Gschneidner, K. A., Jr.; Bünzli, J.-C. G., Pecharsky, V., Eds.; Elsevier: Amsterdam, 2005; Vol. 35, Chapter 225, pp 107–272.

(61) Johnson, C. K. *ORTEP, Report ORNL-5138*, Oak Ridge National Laboratory, Oak Ridge, TN, 1976.

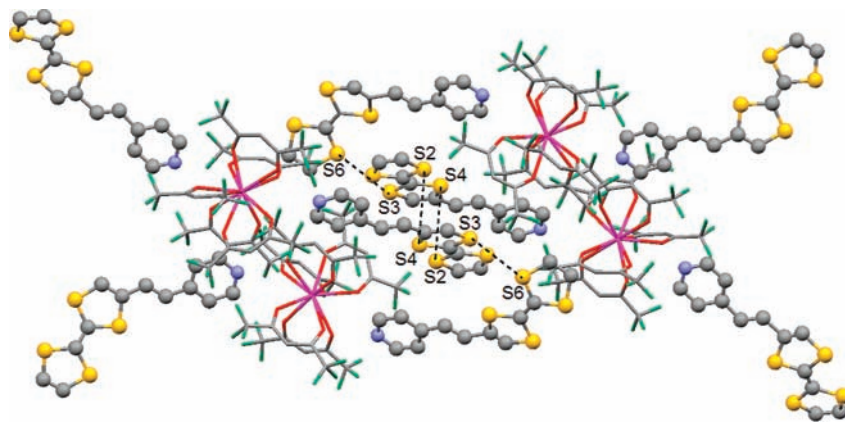


Figure 2. View of the packing of TTF-CH=CH-Py⁺ in **1** showing the inorganic (capped sticks) and organic (balls and sticks) networks along the *c* axis. The shortest S...S contacts are highlighted with dashed lines between the TTF cores.

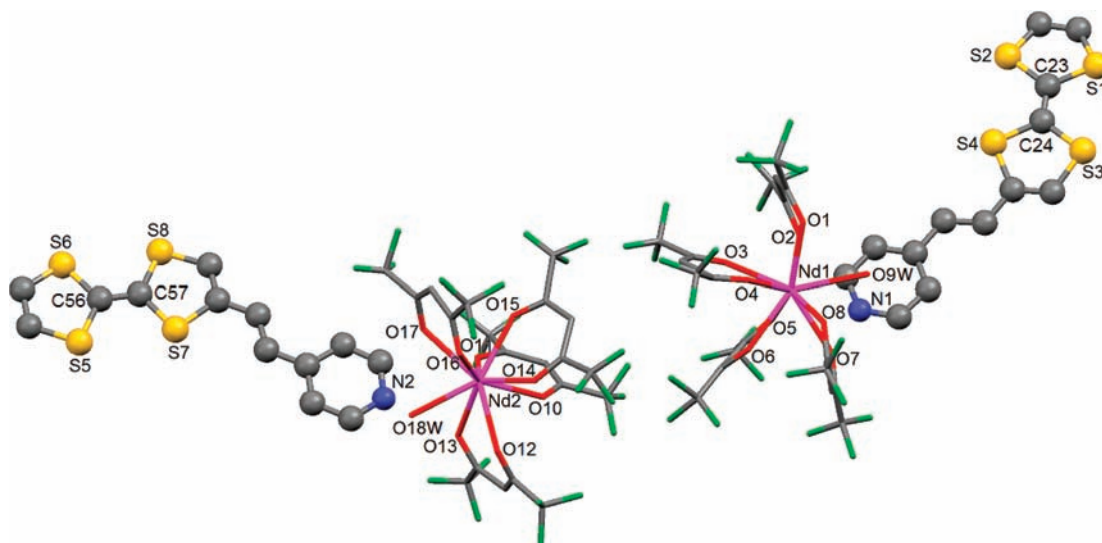


Figure 3. Representation of the asymmetric unit of **2**. The radical cation donors are drawn as balls and sticks; the paramagnetic anionic coordination complexes of Nd(III) are drawn as capped sticks.

interaction. The La-N1 and La-N2 distances are equal to 4.378(8) and 4.409(8) Å, respectively. These distances cannot be considered as coordination bonds because they are longer than covalent La-N bond lengths (2.7–2.8 Å).⁵⁶ The TTF cores stack to form organic networks with the shortest S...S contacts equal to 3.669(6) Å between S3 and S6 (Figure 2). The TTF derivative radicals are almost dimerized with a S2...S4 distance between the dimers equal to 4.176(5). The aromatic systems containing the radical, principally the TTF cores, are not planar, and they are not localized one above the other. The shortest S...S distances are on the order of or longer than the sum of the van der Waals radii of sulfur atoms (3.6 Å), while in the previous reported materials involving lanthanide ions, the S...S contacts are shorter than 3.6 Å.^{48–50} Two reasons can explain the absence of short S...S contacts in **1**: (i) The nitrate and thiocyanate anions in the previously reported structures are smaller than the hexafluoroacetylacetonate. (ii) The TTF-CH=CH-Py⁺ radicals are not free to auto-arrange to build short S...S contacts because the potentially coordinating pyridyl group of each radical interacts with lanthanum. The crystal packing then results from the competition between La-Py and S-S interactions.

$\{[\text{Nd}(\text{hfac})_4(\text{H}_2\text{O})][(\text{TTF}-\text{CH}=\text{CH}-\text{Py}^{+\cdot})]\}_2$ (**2**). Compound **2** crystallizes in the triclinic system, *P*1̄ (No. 2) space group (Table 1). An ORTEP view⁶¹ of the asymmetric unit is depicted in the Figure S2 (Supporting Information). The crystallographic structure of **2** is composed of two monoanionic [Nd(hfac)₄(H₂O)][−] complexes (drawn as capped sticks in Figure 3) and two TTF-CH=CH-Py⁺ derivatives (drawn as balls and sticks in Figure 3). Both monoanionic units and TTF derivatives are crystallographically independent. To ensure the electroneutrality of the structure, both TTF-CH=CH-Py⁺ species must be radical cations. Each Nd(III) ion is surrounded by nine oxygen atoms from four bischelating hfac[−] ligands and one water molecule. The Nd-O distances range from 2.400(7) to 2.569(5) Å. The coordination geometry of the Nd(III) ions can be described as a distorted capped square antiprism. [Nd(hfac)₄(H₂O)][−] complexes related through the inversion center form pseudo-dimeric units with strong hydrogen bonds between water molecules and oxygen atoms of hfac[−] anions (O9w(H)...O1 = 2.893(8), O9w(H)...O8 = 2.906(7), O18w(H)...O12 = 2.961(8), O18w(H)...O16 = 2.911(9)). These dimeric units are identical to that recently described in [N(C₂H₅)₄][Nd(hfac)₄

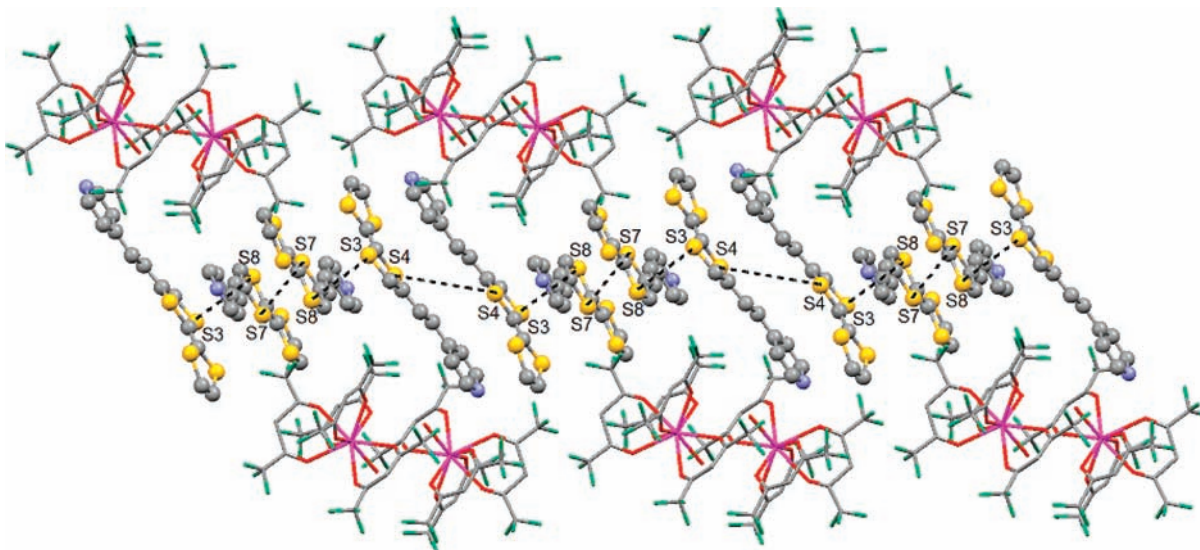


Figure 4. View of the packing in **2** showing the inorganic (sticks) and organic (balls and sticks) networks along the *a* axis. The shortest S...S contacts are highlighted with dashed lines between the TTF cores.

(H₂O)].⁶² The difference is of course the substitution of the [N(C₂H₅)₄]⁺ cation by the TTF-CH=CH-Py^{•+} radical cation. This substitution leads to a shorter intermolecular distance between the two Nd atoms in **2** ($d_{\text{Nd1-Nd1}} = 5.8297(9)$ Å and $d_{\text{Nd2-Nd2}} = 5.7053(9)$; Table 2) than in [N(C₂H₅)₄][Nd(hfac)₄(H₂O)] ($d_{\text{Nd-Nd}} = 5.916$ Å) because of the molecular form difference and steric hindrance between the tetraethylammonium cation and the TTF-CH=CH-Py^{•+} radical cations. Like in **1**, the nitrogen atoms of TTF-CH=CH-Py^{•+} radical cations interact weakly with Nd(III) ($d_{\text{Nd1-N1}} = 4.018(9)$ Å and $d_{\text{Nd2-N2}} = 4.003(8)$ Å), leading to small distortions of the coordination sphere of lanthanide. Thus, the Nd-O distances involving the closest oxygen atoms of the pyridyl moieties (O7, O9w, O13, and O18w) are found to be longer by ca. 0.1 Å than the others. The Nd-N interactions pass through the center of the square face of the coordination polyhedron of Nd(III) ions. Figure 4 shows the crystal packing in **2**, highlighting the inorganic network composed of the pseudo-dimeric unit [(Nd(hfac)₄(H₂O))₂]²⁻ and the organic network, which is composed of stacked TTF-CH=CH-Py^{•+} radical cations. In the organic network, the TTF-CH=CH-Py^{•+} radical cations form columns along the [100] direction. The columns consist of pseudotetrameric units of TTF-CH=CH-Py^{•+} radical cations with short S...S contacts (S3...S8 = 3.741(4) Å and S7...S7 = 3.973(4) Å) slightly longer than the sum of the van der Waals radii. The pseudotetrameric units are separated by long S4...S4 distances (5.518(5) Å). The absence of short S...S contacts has the same origin as in **1**. The aromatic systems containing the radical (mainly the TTF cores) almost fit in parallel planes but are shifted one with respect to the other. In spite of the absence of short S...S interatomic contacts, the π systems overlap. The distance between S3 and the middle of the S7-S8 line of the closest TTF-CH=CH-Py^{•+} radical is equal to 3.537 Å. Such a short distance can lead to strong exchange interactions (Figure S3, Supporting Information).

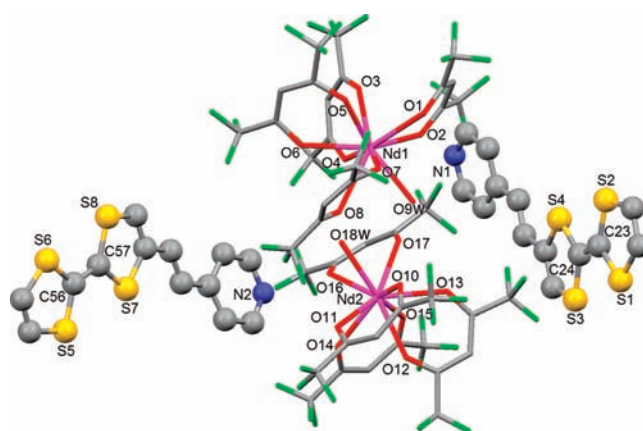


Figure 5. Representation of the asymmetric unit of **3**. The radical cations donors are drawn as balls and sticks; the paramagnetic anionic coordination complexes of Nd(III) are drawn as capped sticks.

{[Nd(hfac)₄(H₂O)][(TTF-CH=CH-Py^{•+})]₂(H₂O)-(C₆H₁₄)_{0.5}} (**3**). Compound **3** crystallizes in the monoclinic system, *P*2₁/*c* (No. 14) space group (Table 1). An ORTEP view of **3** is shown in the Figure S4 (Supporting Information). The asymmetric unit is composed of two [Nd(hfac)₄(H₂O)]⁻ anions (capped sticks), two TTF-CH=CH-Py^{•+} radical cations (balls and sticks), one water molecule of crystallization, and one-half of a hexane (Figure 5). The crystal structure of **3** is similar to the one of **2**. The coordination spheres around the Nd(III) centers consist of four hfac⁻ anions and one water molecule, forming a distorted capped square antiprism. The average Nd-O distance in **3** is 2.485(6) Å and is similar to that in **2** (2.477(6) Å; Table 2). Two anionic units [Nd(hfac)₄(H₂O)]⁻ form a pseudo-dimer like in **2**, but the water crystallization molecule participates in the H-bonding between anionic units. Therefore, the intermolecular distances between the Nd(III) are slightly longer, that is, 6.2253(6) Å, than in **2**. The fundamental difference between the crystal structures **2** and **3** is the arrangement of the TTF-CH=CH-Py^{•+} radical cations. In fact, in **2**, the organic network is made of

(62) Mech, A. *Polyhedron* **2008**, *27*, 393.

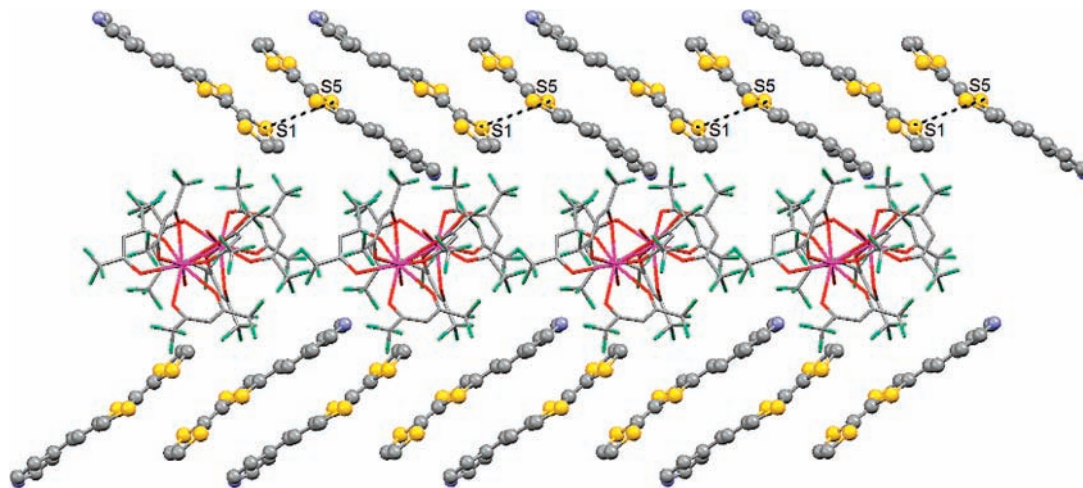


Figure 6. View of the crystal packing of **3** showing the inorganic (sticks) and organic (balls and sticks) networks along the *b* axis. The shortest S...S contacts are highlighted with dashed lines.

tetramers, while it is made of dimers in **3** (Figure 6). The shortest S...S contact (3.824(5) Å) takes place between S1 and S5 (Figure 6) and is longer than the sum of the van de Waals radii, while the mean distance between the planes formed by the six central atoms of the TTF is 3.590(11) Å. Such dimerization leads to a strong overlap between the two π systems of the two TTF cores; therefore, very strong exchange interaction is expected. Each dimer of the TTF-CH=CH-Py^{•+} radical cations is “head-to-tail” stacked, with a donor-acceptor alternation along the [010] direction (Figure 6). The Nd-N distances in **3** are longer than in **2**, with Nd1-N1 and Nd2-N2 distances equal to 4.497(9) and 4.088(9) Å, respectively. The difference in distances between the pyridine moieties of the TTF derivatives and the Nd(III) ions in **3** versus those in **2** can be due to the different stacking of the TTF-CH=CH-Py^{•+} radical cations or the presence of solvent molecules of crystallization.

Photophysical Properties. UV-Visible Absorption Spectroscopy. Solid-state UV-visible absorption spectra of the neutral ligand TTF-CH=CH-Py and compounds **1**, **2**, and **3** are represented in Figure 7 and Figure S5 (Supporting Information). The wavenumbers of the maxima have been determined with four (for TTF-CH=CH-Py) and seven (for complexes) Gaussian deconvolutions of the experimental curve (Figure 7 and Figure S4, Supporting Information). The spectrum of TTF-CH=CH-Py shows four strong absorption bands centered around 38 200, 30 000, 22 900, and 19 900 cm⁻¹. In the TTF donors, the lowest-energy bands of the absorption spectrum are generally assigned to π - π^* charge transfers (CTs) corresponding to the highest occupied molecular orbital (HOMO) \rightarrow lowest unoccupied molecular orbital (LUMO) and HOMO \rightarrow LUMO+*n* single-electron excitations.⁶³ By analogy, in the present case, the HOMO of TTF-CH=CH-Py may be a π orbital centered on the TTF core, whereas the LUMO may be centered on the 4-pyridine moiety.³⁷ The LUMO+*n* represents an acceptor-centered higher-energy orbital than the LUMO. In other words, the lowest-energy transitions correspond to intramolecular charge transfers from the donor TTF core to the acceptor 4-pyridine moiety. The highest-energy transitions (38 200 and 30 000 cm⁻¹) correspond to intramolecular π - π^* transitions of the TTF-CH=CH-Py ligand. Spectra of **1**, **2**, and **3** are very similar (Figure 7 and

Figure S5, Supporting Information). They show three new absorption bands compared to the spectrum of the neutral TTF-CH=CH-Py ligand. On one hand, they show an intense absorption band centered at 33 000 cm⁻¹ (red deconvolution) principally due to intramolecular π - π^* transition of the hfac⁻ anions.⁶² On the other hand, the apparition of two absorption bands at 16 000 cm⁻¹ (CT₁) and 26 500 cm⁻¹ (CT₂) (blue deconvolutions) is noted. These charge transfers are characteristic of oxidized TTF derivatives⁶³ and confirm the radical form of the TTF-CH=CH-Py in our compounds. By analogy with previous works,⁶³ the band centered at 16 000 cm⁻¹ can be attributed to an intramolecular charge transfer of one electron from a SOMO-*n* localized on the 4-pyridine group to the SOMO localized on the TTF^{•+} fragment. The SOMO-*n* is a lower-energy orbital than the SOMO. The absorption band centered at 26 500 cm⁻¹ is attributed to the SOMO \rightarrow LUMO transition of the TTF-CH=CH-Py^{•+} radical cation. This latter transition is analogous to the HOMO \rightarrow LUMO transitions of the neutral TTF-CH=CH-Py. The intermolecular electronic interactions with the anionic lanthanide complexes have been considered to play a negligible role in the interpretation of the UV-visible absorption spectroscopy.

Luminescence Properties for 2. The Nd³⁺ luminescence is observed upon excitation in the entire spectrum up to 14 300 cm⁻¹, and an additional broad organic fluorescence band is observed mainly by irradiation in the CT₁ transition (Figure 8). The Nd(III) luminescence is composed of the classic three emission bands localized at 11 070 (⁴F_{3/2} \rightarrow ⁴I_{9/2}), 9400 (⁴F_{3/2} \rightarrow ⁴I_{11/2}), and 7470 (⁴F_{3/2} \rightarrow ⁴I_{13/2}) cm⁻¹, while the fluorescence band of the radical cation is centered at 10 200 cm⁻¹ (relaxed CT₁ \rightarrow ground state). Higher-energy excitation (25 000 cm⁻¹) (corresponding to the CT₂ and intramolecular transition of the 4-pyridine substituent) leads to a significant decreasing of the fluorescence band of the organic radical cation (Figure 8). It is worth noticing that similar Nd(III) luminescence is observed with excitation of the [NET₄][Nd(hfac)₄] anion due to the presence of a large

(63) Jia, C.; Liu, S.-X.; Tanner, C.; Leiggener, C.; Neels, A.; Sanguinet, L.; Levillain, E.; Leutwyler, S.; Hauser, A.; Decurtins, S. *Chem.—Eur. J.* **2007**, *13*, 3804.

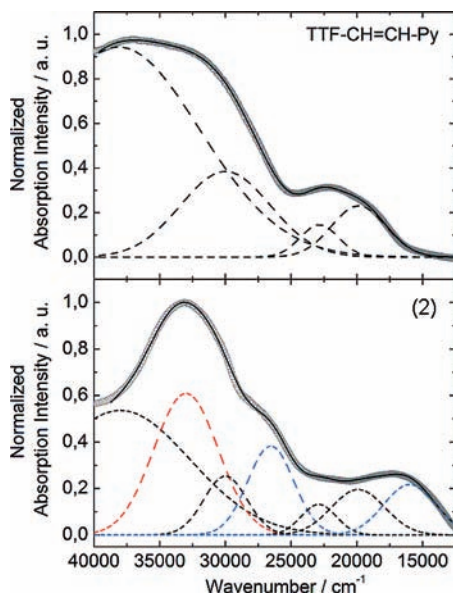


Figure 7. Experimental solid-state (KBr pellets) UV–visible absorption spectra of TTF–CH=CH–Py and **2** (open circles), deconvolution of the experimental curve (dashed lines), and the best fit $R = 0.9999$ (for TTF–CH=CH–Py) and $R = 0.9996$ (for **2**).

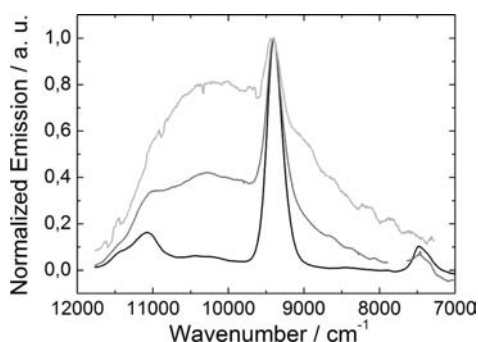


Figure 8. Emission spectra of **2** in the near-IR (curve in black for $\lambda_{\text{ex}} = 25000 \text{ cm}^{-1}$, in gray for $\lambda_{\text{ex}} = 15625 \text{ cm}^{-1}$, and in light gray for $\lambda_{\text{ex}} = 14300 \text{ cm}^{-1}$) at room temperature (293 K) in the solid state.

number of f–f transitions in the $25000\text{--}14300 \text{ cm}^{-1}$ spectral range.⁶² These transitions are forbidden and feature a very low extinction coefficient, but in the solid state, the concentration is high enough to allow this direct luminescence sensitization process. Therefore, it is not possible to conclude that, in **2**, neodymium luminescence is sensitized through an antenna effect from the radical-cation-centered charge-transfer transition as recently observed for Eu(III), but also Yb(III) and Nd(III) luminescence,^{64,65} or by a direct process through the f–f transitions.

EPR Measurements. The EPR spectra of single crystals of **1** (at 225 and 70 K) and **2** (at 70 K) are shown in Figure S6 (Supporting Information). These spectra show a weak and broad signal centered at the isotropic g value ($g = 2.008$) typical of a radical cation TTF derivative.^{38,66} The signal of the paramagnetic Nd(III) ion is not observed

(64) Yang, C.; Fu, L.-M.; Wang, Y.; Zhang, J. P.; Wong, W.-T.; Ai, X.-C.; Qiao, Y. F.; Zou, B.-S.; Gui, L.-L. *Angew. Chem., Int. Ed.* **2004**, *43*, 5010.

(65) D'Aléo, A.; Picot, A.; Beeby, A.; Williams, J. A. G.; Le Guennic, B.; Andraud, C.; Maury, O. *Inorg. Chem.* **2008**, *47*, 10258.

(66) Scout, J. S. In *Highly Conducting Quasi-One-Dimensional Organic Crystals*; Conwell, E., Ed.; Academic Press: New York, 1988; Semiconductors and Semimetals, Vol. 27, pp 385–436.

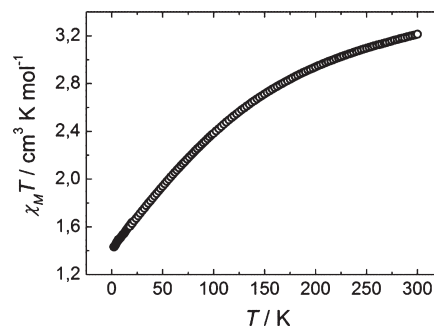


Figure 9. Thermal dependence of the product $\chi_M T$ of a powdered sample of **2**.

for temperatures higher than 70 K. The two spectra of **1** at 70 and 225 K are similar. The presence of a weak signal at 70 K indicates that the TTF–CH=CH–Py^{•+} radicals are almost completely antiferromagnetically coupled at this temperature. The intensity of the signal is in agreement with a dimerization and tetramerization of the TTF derivatives in the crystal structures of **1** and **2**, leading to strong antiferromagnetic interactions between the radical cations. The EPR measurements of **3** around 70 K show no signal due to the total dimerization of the TTF derivatives leading to strong antiferromagnetic exchange interaction between the π electrons.

Magnetic Properties. $\{[\text{La}(\text{hfac})_3][(\text{TTF}-\text{CH}=\text{CH}-\text{Py}^{\bullet+})_2]\}$ (**1**). The magnetization of **1** has been measured between 2 and 300 K. As expected, it shows quasi-diamagnetic behavior. This behavior is in agreement with the association of a diamagnetic $4f^0$ La(III) ion and dimerized TTF radical cations.

$\{[\text{Nd}(\text{hfac})_4(\text{H}_2\text{O})][(\text{TTF}-\text{CH}=\text{CH}-\text{Py}^{\bullet+})_2]\}$ (**2**) and $\{[\text{Nd}(\text{hfac})_4(\text{H}_2\text{O})][(\text{TTF}-\text{CH}=\text{CH}-\text{Py}^{\bullet+})_2](\text{H}_2\text{O})(\text{C}_6\text{H}_{14})_{0.5}\}$ (**3**). The magnetic properties for **2** and **3** are almost identical, and only one scientific discussion is given with, in square brackets, the corresponding values of **3** for comparison. The thermal dependence of the $\chi_M T$ products for **2** and **3** are respectively shown in Figure 9 and Figure S7 (Supporting Information). The $\chi_M T$ versus T curve shows a monotonic decrease from 300 to 2 K. The room-temperature value of $\chi_M T$ is equal to $3.21 [3.19] \text{ cm}^3 \text{ K mol}^{-1}$, while it is equal to $1.43 [1.46] \text{ cm}^3 \text{ K mol}^{-1}$ at 2 K. The electronic configuration $4f^3$ is split into spectroscopic terms ^{2S+1}L by interelectronic repulsions, and the highest spin multiplicity term (4I) is the lowest in energy. Each term ^{2S+1}L is split into spectroscopic levels $^{2S+1}L_J$ by spin–orbit coupling with $|L - S| \leq J \leq L + S$. The ground state of Nd(III) is then $^4I_{9/2}$, with a Zeeman factor $g_{9/2}$ equal to $8/11$.⁶⁷ Finally, each $^{2S+1}L_J$ term is split by crystal field into Stark sublevels separated by around 100 cm^{-1} .⁶⁸ This splitting is smaller than for first transition metallic ions because the 4f orbitals are not involved in the first approximation in the bonds with neighboring atoms. In addition, the energy splitting between the ground state $^4I_{9/2}$ and the first excited state $^4I_{11/2}$ is equal to 1670 cm^{-1} . So at room temperature, only the Stark sublevels from the $^4I_{9/2}$ ground state are populated. When the temperature decreases, the depopulation of these

(67) Benelli, C.; Gatteschi, D. *Chem. Rev.* **2002**, *102*, 2369.

(68) Sutter, J.-P.; Kahn, M. L. *Magnetism: Molecules to Materials V*; VCH: Weinheim, Germany, 2005.

sublevels leads to a deviation from the Curie law observed by a variation of the $\chi_M T$ product, even in the absence of any exchange interaction. The room-temperature value of $\chi_M T$ is in agreement with the expected value for two isolated Nd(III) ions in a NdO9 crystal field (the theoretical value is $3.20 \text{ cm}^3 \text{ K mol}^{-1}$).^{57,69} No contribution of the radical cations ($s = 1/2$) is observed, and the decrease of the $\chi_M T$ product is only due to the crystal field effect. The absence of a contribution of the spin of the radical cations supports the observation or the nonobservation of weak signals of the organic radicals on EPR spectra.

Conductivity. The electrical resistivity of single crystals of **1**, **2**, and **3** has been measured between 300 and 70 K using the standard two-probe method. Gold wires were attached to the crystal with carbon paste. The values of resistivity are close to $10 \text{ k}\Omega \text{ cm}^{-1}$ for all of the materials, and they can be described as insulators in this temperature range. These experimental observations are in agreement with the crystal structures (dimers or tetramers) and the oxidized state +1 of all donors.

Conclusions

In this paper, the three first tetrathiafulvalene radical cation salts of poly(hexafluoroacetylacetonate)lanthanide are obtained by a spontaneous oxidation in the presence of the lanthanide precursors. All of the crystal structures have been determined by single-crystal X-ray diffraction. The lanthanide centers are surrounded by 10 or 9 oxygen atoms, and their coordination geometries can be described as a tetracahe-dron or distorted capped square antiprism polyhedron, respectively, for La(III) and Nd(III) ions. The lattices consist of an inorganic network composed of the dianionic penta(1,1,1,5,5,5-hexafluoroacetylacetonate)La(III) (for **1**), a

dimer of tetra(1,1,1,5,5,5-hexafluoroacetylacetonate)Nd(III) (for **2** and **3**), and an organic network composed by the 4-(2-tetrathiafulvalenyl-ethenyl)pyridine radical cations. The radical form of the donors has been confirmed with absorption UV–visible–NIR spectroscopy and EPR measurements. Short contacts between sulfur atoms of the donors are observed, leading to strong antiferromagnetic interactions and a quasi-diamagnetic behavior of the organic network. Nd(III)-based compounds are paramagnetic due to the magnetic properties of the Nd(III) centers. Both organic and inorganic networks interact through intermolecular interactions between the nitrogen atoms of the pyridine moieties and the lanthanides. Typical near-infrared luminescence of Nd(III) (9400 cm^{-1}) has been observed for **2** without quenching of the luminescence by the TTF–CH=CH–Py radical cations. The fluorescence of the latter has also been observed at a wavenumber of $10\,200 \text{ cm}^{-1}$. Compound **2** demonstrates that it is possible to employ near-infrared luminescent lanthanides to elaborate luminescent TTF-based compounds. The incorporation of other donors and near-infrared luminescent lanthanides is in progress in our laboratory to elaborate on luminescent magnetic conducting materials.

Acknowledgment. This work was supported by the CNRS, MAGMANet European excellence network, Université de Rennes 1, and Région Bretagne.

Supporting Information Available: CIF files for {[La(hfac)₅]-[(TTF–CH=CH–Py^{•+})]₂} (**1**), {[Nd(hfac)₄(H₂O)][(TTF–CH=CH–Py^{•+})]₂} (**2**), and {[Nd(hfac)₄(H₂O)][(TTF–CH=CH–Py^{•+})]₂(H₂O)(C₆H₁₄)_{0.5}} (**3**). ORTEP view for **1** (Figure S1), **2** (Figure S2), and **3** (Figure S4). Overlap between the donors for **2** (Figure S3). UV–visible–NIR absorption spectra for **1** and **3** (Figure S5). Figure of EPR for **1** and **2** (Figure S6). $\chi_M T(T)$ curve for **3** (Figure S7). This material is available free of charge via the Internet at <http://pubs.acs.org>.

(69) Kahn, O. *Molecular Magnetism*; VCH: Weinheim, Germany, 1993.